Original Article

Journal of Tissue Engineering
Volume 10: 1–12
© The Author(s) 2019
Article reuse guidelines:
sagepub.com/journals-permissions
DOI: 10.1177/2041731419843710
journals.sagepub.com/home/tej
SAGE

Microarchitectural analysis of decellularised unscarred and scarred dermis provides insight into the organisation and ultrastructure of the human skin with implications for future dermal substitute scaffold design

Umair Khan[1,2] and Ardeshir Bayat[1]

Abstract

The three-dimensional spatial arrangement of dermal tissue plays a crucial role in directing cellular behaviour during wound healing. It is vital to elucidate a better understanding of the three-dimensional dermal architecture of human skin. We sought to understand the configuration in morphological structure of decellularised human dermis between unscarred skin and normotrophic scars. Skin biopsies underwent decellularisation (DNA removal = 88%). Histological analysis showed no change in gross morphology of decellularised unscarred and scarred dermis. Multiphoton and atomic force microscopies showed that collagen fibres in unscarred decellularised dermis were interwoven akin to a mesh-like structure. Collagen fibres in decellularised unscarred dermis were less stiff (mean: 2.155 ± 0.9595 MPa; $p < 0.0001$) with a rougher ($R_q = 16.5$, $R_a = 12.5$, $R_{max} = 198$; $p < 0.0001$) surface topography. Scarred dermis had a higher collagen volume density (papillary dermis, $p < 0.0082$; reticular dermis, $p < 0.0332$). The results demonstrate that scaffolds should exhibit a mesh-like structure with a biomimetic surface and low stiffness.

Keywords

Skin, decellularised, scarred, unscarred, architecture, ultrastructure, collagen fibre orientation, biomimetics

Date Received: 9 December 2018; accepted: 22 March 2019

Introduction

Wound healing is a normal dynamic reciprocal overlapping process that depending on the depth of cutaneous dermal injury usually can lead to permanent scar formation.[1] In most cases, this is normotrophic scarring but, in some cases, it can result in pathological scarring such as atrophic, hypertrophic or keloid scars.[1] To date, pathological scarring has been studied extensively.[2] However, despite the technological advances that have led to a greater understanding of the molecular basis of cutaneous wound healing, our understanding of the morphological alterations from unscarred skin to normotrophic scar formation still remains unclear.[3,4] More recently, studies have highlighted the crucial role the dermal tissue plays in normotrophic scar formation.[5] In their study on the mechanism of scar formation,[5] it was suggested that the formation of a normal

[1]Plastic and Reconstructive Surgery Research, Division of Musculoskeletal & Dermatological Sciences, NIHR Manchester Biomedical Research Centre, Manchester Academic Health Science Centre, The University of Manchester, Manchester, UK
[2]Manchester University NHS Foundation Trust, Manchester, UK

Corresponding author:
Ardeshir Bayat, Plastic and Reconstructive Surgery Research, Division of Musculoskeletal & Dermatological Sciences, NIHR Manchester Biomedical Research Centre, Manchester Academic Health Science Centre, The University of Manchester, Stopford Building, Oxford Road, Manchester M13 9PL, UK.
Email: ardeshir.bayat@manchester.ac.uk

scar may be related to the loss of integrity of the intact dermal architecture, that is, the loss of collagen network, thus highlighting the crucial role this structure plays in regulating cellular behaviour during the process of cutaneous wound healing. Collagen acts not only as a benign scaffold, but also as a dynamic structure that plays a crucial role in tissue function and in defining, within the cellular microenvironment, the regulatory behaviour of resident and migratory cells during wound healing.[6–9] Therefore, when the integrity of this scaffold is compromised during cutaneous injury, especially deep dermal injuries, it cannot effectively mediate cellular behaviour and consequently leads to scar tissue generation.[5,10] Morphologically, this leads to the formation of an irregularly arranged fibrous tissue.[5]

Presently, several approaches have been developed for tissue engineering skin substitutes in order to achieve a specific functional objective.[11] However, because of the limited three-dimensional (3D) understanding of the native dermal extracellular matrix (ECM), so far these engineered skin substitutes fail to fulfil the criteria for a fully functional skin.[12] The physical properties of engineered scaffolds influence the interaction and behaviour of cellular components during wound healing. Size of pores, specific shapes formed virtually between neighbouring adhesion sites and angles formed between fibres all can influence the migratory behaviour of dermal fibroblasts.[13] Engineered dermal scaffolds that resemble the native microarchitecture of unscarred skin may therefore play a crucial role in wound healing, thus preventing the formation of excessive scar tissue.

Decellularised tissues and organs have recently emerged as an alternative to synthetic biomaterials. However, the presence of even minimal cells in human tissue allografts can stimulate an immune response, consequently resulting in rejection of the implanted allograft by the recipient. Thus, to overcome this, several groups have developed decellularised bioscaffolds with the intention of recellularisation in order to regenerate tissues and organs.[14] Bioscaffolds have widely been developed for a number of organs; however, to date, the structural and mechanical characteristics of scaffolds for dermal regeneration have not been fully identified.

Furthermore, over the last few decades, the published literature has highlighted that patients exhibit significant psychological distress even in the presence of minimal scarring, especially following minor facial lacerations.[15–17] This is irrespective of the scar type[15,16] and thus highlights the fact that even minimal improvements in normotrophic scar appearance can significantly improve the psychosocial quality of life for these patients.

To our knowledge, for the first time, decellularisation of scarred human dermis was achieved using a process originally developed to decellularise a wide range of tissues, including heart valves,[18,19] meniscus, pericardium, femoral arteries[20] and the amniotic membrane.[21] In our study, we amended and optimised the process for decellularisation of scarred human dermis. We performed qualitative and quantitative analyses of our decellularised scarred dermis, carefully considering various parameters that are necessary when engineering dermal scaffolds, and which may influence the cellular compartment during cutaneous wound healing.

Materials and methods

Tissue samples

Ethical approval was obtained from male Caucasian subjects undergoing elective cosmetic abdominoplasty surgery with appropriate ethical committee and Human Tissue Authority approval (16/NW/0736 IRAS 214160). A total of six full-thickness skin tissue samples approximately 7 cm by 4 cm (three unscarred and three normal cutaneous scars) were collected from three separate patients (aged 37, 42, and 54 years). Immediately following excision, the tissue samples were snap-frozen using dry ice, placed in polypropylene tubes and stored in a −80°C freezer until further use.

Decellularisation

Reagents. All reagents used in this study were highest-grade research products formulated for human skin decellularisation specifically and strictly conformed to Good Manufacturing Practice (GMP) standards (Table 1).

Protocol. Non-processed fresh skin was thawed at room temperature. The skin samples were immersed in Cambridge Antibiotic Solution (nystatin, vancomyin HCl, gentamicin sulphate, polymyxin B sulphate, imipenem) and incubated with agitation on an orbital shaker (200 r/min). The tissue specimens were then washed three times with agitation (200 r/min) using phosphate-buffered saline (PBS). Next, we removed the epidermis by placing the specimens in de-epidermalising buffer plus 1% penicillin/streptomycin solution (10 mL/L). After 18 h of incubation at room temperature, we removed the epidermis using forceps. The dermal tissue was washed immediately with Dulbecco's phosphate-buffered saline (dPBS) plus 1% penicillin/streptomycin solution (10 mL/L) and 10 KIU/mL aprotinin (1 mL/L). The cellular dermis was then placed into hypotonic buffer plus 1% penicillin/streptomycin solution (10 mL/L) and 10 KIU/mL aprotinin (1 mL/L) for 24 h at 4°C with agitation (200 r/min). Next, the samples were transferred into detergent buffer plus 1% penicillin/streptomycin solution (10 mL/L) and 10 KIU/mL aprotinin (1 mL/L), and agitated (200 r/min) at room temperature. After 24 h, the dermal tissues were washed at room temperature for 20 min in a pot containing dPBS plus

Table 1. Source of reagents.

Buffer	Supplier	Catalogue No.
Cambridge Antibiotic Solution	Source BioScience	04-301
dPBS (w/o calcium chloride, w/o magnesium chloride)	Sigma-Aldrich	D8537
10% formalin solution, neutral buffered	Sigma-Aldrich	HT501320
De-epidermalising solution – 1 L dH_2O, 58.44 g NaCl (1M). Autoclave.	Source BioScience	04-332
Hypotonic Buffer Base – 1 L dH_2O, 1 g EDTA (0.1%), 1.211 g TRIS (10 mM). pH 8.0. Autoclave. Stored at 4°C.	Source BioScience	04-333
Nuclease Buffer Base – 6.055 g TRIS (50 mM), 2.033 g $MgCl_2$ (10 mM). pH 7.5.	Source BioScience	04-335
Wash Buffer Base – 1 L PBS, 1 g EDTA (0.1%). pH 8.5. Autoclave.	Source BioScience	04-331
Detergent Buffer Base – 1 L dH_2O, 1 g EDTA (0.1%), 1.211 g TRIS (10 mM), 0.1 g SDS (0.01%). pH 8.0. Autoclave. Stored at 4°C.	Source BioScience	04-334
Penicillin–streptomycin solution	Sigma-Aldrich	P4333
Benzonase	Merck Millipore	71206-3
Aprotinin (10,000 KIU/mL) BP	Nordic Pharma	N/A

dPBS: Dulbecco's phosphate-buffered saline; EDTA: ethylenediaminetetraacetic acid; TRIS: tris(hydroxymethyl)aminomethane; PBS: phosphate-buffered saline; SDS: sodium dodecyl sulphate.

1% penicillin/streptomycin solution (10 mL/L) and 10 KIU/mL aprotinin (1 mL/L). Following three separate washes, the dermis was immersed at 37°C in nuclease buffer plus 1% penicillin/streptomycin solution (10 mL/L), 10 KIU/mL aprotinin (1 mL/L) and 1 U/mL benzonase. The activity of benzonase was checked prior to usage according to manufacturer instructions. After 3 h, the tissues were immediately washed in wash buffer base for 20 min at room temperature with agitation (200 r/min). The decellularised dermis (DCD) was then either stored in a −80°C freezer or fixed in 10% formalin.

Analysis of DCD

Samples of DCD were analysed to validate the process. The analysis involved histological evaluation and quantification of residual DNA content. Furthermore, nanomechanical and morphological analysis of cellular and decellularised dermis was performed using atomic force microscopy (AFM) and multiphoton microscopy (MPM). In all the analyses, samples of DCD were compared with control samples of either intact skin or cellular dermis, unless otherwise stated. Intact skin is described as the tissue that has not been subjected to the decellularisation process. A total of six tissue specimens were analysed (three unscarred and three scarred) for each test.

Histology. Samples of intact skin and cellular and decellularised dermis were paraffin-embedded on a tissue processor after fixing in 10% formalin for 48 h. The wax blocks were cut into 10-μm sections using a microtome and dewaxed by incubating twice into xylene for 5 min. Sections were subsequently dehydrated in a graded ethanol series (100%, 90%, 70%, 50%) and finally rehydrated by placing into distilled water for 2 min. The sections were stained with haematoxylin and eosin (H&E) and observed under a light microscope to evaluate the histoarchitecture. DAPI (4′,6-diamidino-2-phenylindole) dye (Sigma, UK) was used to visualise nuclear material under a fluorescent microscope. Fixed sections were washed three times in PBS. Next 300 nM DAPI stain solution was used to cover the samples. Sections were incubated for 3 min and protected from light. The stain solution was then removed and the sections were washed thoroughly three times in PBS to remove unbound DAPI. ImageJ and CellProfiler were used to analyse the DAPI stains.

DNA quantification. A commercially available genomic DNA isolation kit (Easy-DNA™; Invitrogen, UK) was used to quantify DNA levels before and after decellularisation. Punch biopsies (5 mm) were obtained from cellular and decellularised unscarred human dermis. Tissue samples were blotted dry, weighed and processed according to manufacturer's instructions. Levels of isolated DNA were quantified using the Quant-iT PicoGreen dsDNA reagent kit (Invitrogen) and measured using a fluorescence microplate reader. The excitation and emission wavelengths of 480 and 520 nm, respectively, were used. The amount of DNA remaining in decellularised unscarred and scarred human dermis was calculated as the percentage of DNA within the cellular dermis (considered 100%) from the same donor.

Functional testing with AFM

Sample preparation. Samples of both unscarred and scarred DCD were transferred from the −80°C freezer into an optical cutting temperature (OCT) compound for cryosectioning. The frozen blocks were placed on metal chucks and sectioned with 10 μm thickness using a cryostat, and subsequently the sections were stored in the −80°C freezer. At 24 h prior to use, the cryosections were brought to room temperature and washed multiple times

for different durations (5, 3, 2 and 1 min) with distilled water and left to dry overnight.

AFM scanning. The 5-μm scans were captured from cryosections (prepared as described above) using a Bruker Catalyst AFM (Coventry, UK) mounted on a Nikon Eclipse Ti. The system was controlled using a Bruker NanoScope V controller interfaced via the Bruker NanoScope software (V9.1). Using the AFM optical microscope, the cantilever tip was moved 100 μm below the epidermal basement membrane into the papillary dermis for both unscarred and scarred tissue. Note that the epidermis was not present as it was removed as part of the decellularisation process. Typical AFM tapping mode images were captured in air 100 μm below the depth of the epidermal basement membrane in the papillary dermis, using ScanAsyst™ mode and ScanAsyst-Air cantilevers (nominal spring constant = 0.4 N/m and radius of curvature = 5 nm; Bruker AXS S.A.S, France). Image analysis, including collagen D-banding and roughness value extraction, was performed using the Bruker NanoScope analysis software (V1.5). Three common quantitative parameters of surface roughness were obtained. The mean roughness (R_a) is the arithmetic mean of the absolute values of the roughness profile coordinates in the plane of the surface and is expressed as

$$R_a = \frac{1}{N}\sum_{j=1}^{N}\left|Z_j\right|$$

The root mean square roughness (R_q) is the root mean square average of height deviations from the roughness profile coordinates and is expressed as

$$R_q = \sqrt{\frac{\sum Z_i^2}{N}}$$

The maximum roughness depth (R_{max}) is the largest single roughness depth within the plane of evaluation. The potential wear of the AFM tip from prolonged usage was considered non-detrimental to the surface roughness quantification.

Mechanical testing. Cryosections (prepared as described previously) were used to obtain the elastic modulus values for both decellularised unscarred dermis and scarred dermis. Nanomechanical analysis was performed using the Bruker Catalyst system described above and a pyramidal probe mounted on a springboard cantilever (CP-FM-BSG-A-sQube, Germany). Microscopic slides with the skin samples were placed on the sample stage of the Bruker Catalyst system with indentation performed in air. The spring constant (3.832 N/m) and deflection sensitivity (unscarred dermis = 2.15 nm/V, scarred dermis = 3.75 nm/V) for the cantilever were calculated by standard methodology. The cantilever tip was moved into the papillary dermis, 100 μm below the epidermal basement membrane. A total of 100 force curves were obtained from three locations within the papillary dermis of each tissue type using a ramp size of 1 μm and a trigger threshold of 100 nm, which falls within the 2% maximum depth to avoid substrate contribution. The area covered for each location was 4 μm (2 μm × 2 μm). The three areas sampled were similar in location between both unscarred and scarred papillary dermis, such that areas 1, 2 and 3 of unscarred DCD corresponded to areas 1, 2 and 3 of scarred DCD. Curves were analysed using the Bruker NanoScope Analysis software and the elastic modulus values for each curve were obtained using the following formula

$$F = \frac{2}{\pi}\left(\frac{E}{1-\nu^2}\right)h^2 \tan\alpha$$

Here, F is the force from the force curve, E is the elastic modulus, ν is Poisson's ratio (taken to be 0.5), h is the indentation depth and α is the half angle of the AFM probe (taken to be 36° according to the manufacturer). The half angle was confirmed during standardisation of the spring constant.

Structural evaluation using MPM

Sample preparation. Immediately after de-epidermalisation and complete decellularisation, samples of cellular and decellularised dermis of both unscarred and scarred tissue were transferred into the OCT compound for cryosectioning. The tissue sections for MPM were cut into 30 μm thickness and sandwiched between a microscopic slide and a cover slip. The sections were processed with the cover slip facing the microscope objective. Furthermore, a small amount of PBS was dripped into the tissue specimen to avoid sample dehydration or shrinkage during the scanning process.

MPM scanning. Images were collected on a high-throughput scanning Leica SP8 Upright multiphoton microscope (Leica, UK) using a 25×/0.95L HC Fluotar dipping objective and 3× magnification. The settings are as follows: scan speed – 1000 Hz unidirectional and format – 512 × 512 pixels. Images were collected using a hybrid detector with a fixed filter and with two-photon excitation using a Mai Tai MP Ti:Sapphire laser (Spectra-Physics, UK) tuned to an excitation wavelength of 810 nm and using 15% of maximum power. In this study, a single channel was employed to obtain the high-contrast images of collagen in the dermis of unscarred and scarred tissue, both pre- and post-decellularisation. The channel corresponded to the wavelength range of 398–409 nm to show the microstructure of collagen using second harmonic generation (SHG) signals. In order to increase the contrast of the SHG images, the collagen images were colour-coded in green. Images were collected sequentially from superficial to deep dermis. When acquiring 3D optical stacks, the multiphoton software Imaris (V1.8.0) was used

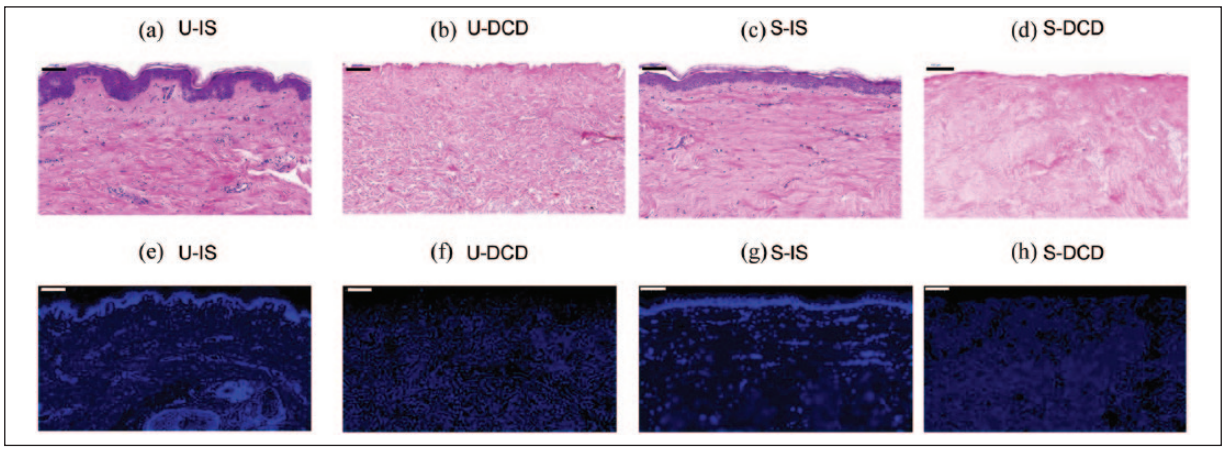

Figure 1. Histological sections of unscarred and scarred tissue. Longitudinal sections were stained with haematoxylin and eosin (a–d) and DAPI (e–h) to visualise the general tissue morphology and nuclear material, respectively. Scale bars: 100 μm.
U-IS: unscarred intact skin; U-DCD: unscarred decellularised dermis; S-IS: scarred intact skin; S-DCD: scarred decellularised dermis.

to determine the optimal number of Z sections. Only the maximum intensity projections of these 3D stacks were used for quantification purposes.

Quantification of collagen volume density. Sequential two-dimensional (2D) images of 2-μm interval of the superficial and deep dermis of unscarred and scarred tissue were obtained with an area of 512 × 512 pixels, up to a final depth of 40 μm, resulting in a total of 20 images per tissue sample analysed. For each individual tissue, an average of five random fields were analysed with an area of 512 × 512 pixels in both the papillary and reticular dermis. This stack of 2D images was used to reconstruct a 3D multiphoton image of collagen. The following method was employed to quantify collagen volume density. The pixel number of collagen SHG image and the total pixel number within the superficial and deep dermis were calculated using the Imaris software. Then the volume density of collagen was calculated by dividing the pixel number of collagen SHG signal by the total pixel number within the region.

Statistical analysis

Statistical analysis of experimental data was performed using paired *t*-test and repeated-measures one-way analysis of variance (RM-OW-ANOVA). All statistical analyses were performed using GraphPad Prism software. The results are expressed as mean ± standard deviation (SD), unless stated otherwise. Two-tailed *p* values less than 0.05 were considered statistically significant.

Results

The entire decellularisation process took approximately 5 days to complete, due to several incubation times for epidermal removal, hypotonic and detergent buffer steps.

Histology

In unscarred skin (Figure 1(a)), the rete ridges projecting into the underlying dermis were clearly visible. These epithelial extensions were not visible within scarred tissue (Figure 1(c)). There was no evidence of cellular material observed in sections of DCD stained with H&E (Figure 1(b) and (d)), and furthermore there were no obvious differences in ECM morphology between cellular and decellularised dermis of each tissue type.

Residual DNA analysis

DAPI staining demonstrated the presence of nuclear material in intact unscarred and scarred skin (Figure 1(e) and (g)), but not in DCD of either tissue (Figure 1(f) and (h)). Only background autofluorescence was present in DCD. A mean of 11.9% DNA was observed, equivalent to 88.1% removal in unscarred dermis, and a mean of 9.9% DNA was observed in scarred dermis (Table 2).

Structural analysis using AFM

For illustration purposes, images from a single patient aged 42 years were representatively demonstrated (Figure 2). There is an irregular and random orientation of collagen fibres in unscarred DCD (Figure 2(b1)–(b3)). Tightly packed fibres with a strong degree of orientation were observed in decellularised scarred dermis (Figure 2(b4)–(b6)). There is evidence of structural damage to the collagen in unscarred dermis (Figure 2(b1) and (b3)); however, this is not observed in the scarred dermis (Figure 2(b4) and (b6)). This is possibly due to the detergents used in our decellularisation protocol. Further studies are needed to elucidate whether detergents are responsible for this 'wrinkling' effect observed in the unscarred dermis and whether further optimisation of our decellularisation protocol is

Table 2. Comparison of DNA content in cellular and decellularised unscarred and scarred dermis.

Sample	Donor	Biopsy weight (mg)	Total DNA (ng)	DNA/tissue (ng/mg)	%DNA remaining
Unscarred cellularised dermis	1	15	2.21	0.15	100
	2	21	2.30	0.11	100
	3	18	2.66	0.15	100
Unscarred decellularised dermis	1	15	0.31	0.02	13.3
	2	23	0.18	0.01	9.1
	3	17	0.27	0.02	13.3
Scarred cellularised dermis	4	19	2.51	0.13	100
	5	23	3.26	0.14	100
	6	22	2.85	0.13	100
Scarred decellularised dermis	4	19	0.28	0.01	7.7
	5	22	0.35	0.02	14.3
	6	21	0.15	0.01	7.7

required. The characteristic D-banding of collagen fibres (–67 nm) was resolved for both unscarred and scarred dermis. The banding pattern along the straight line between two cross points (Figure 2(b2) and (b5)) of a single collagen fibre was analysed, giving a periodic repeat of 65 ± 3.61 nm and 69 ± 2.49 nm, respectively, for decellularised unscarred and scarred dermis (Table 3).

The surface of collagen fibres in unscarred DCD appears rougher compared to decellularised scarred dermis (Figure 2(c) – unscarred: $R_q = 16.5$, $R_a = 12.5$, $R_{max} = 198$; scarred: $R_q = 8.93$, $R_a = 6.9$, $R_{max} = 96.9$). A significant difference was present between each corresponding roughness parameter for both tissue types ($p < 0.0001$). There was a greater variation in surface topography of collagen fibres in unscarred DCD.

Mechanical testing using AFM

The distributions of elastic moduli are distinctively different, both numerically and in their shape for unscarred and scarred DCD (Figure 3(a)). Overall, there is a significant difference between the elastic moduli of unscarred and scarred DCD, with scarred tissue appearing stiffer. The box and whisker plot indicates the interquartile ranges, maximums, minimums, and medians. There is a reduced variation in fibre stiffness in unscarred dermis with less spread of the data between the upper and lower quartiles. Furthermore, because of the sample volume limited to three for each tissue type, the number of force curves ($n = 300$) needed to be high for the data to be representative. This is reflected in the wide range of reduced modulus values as shown by the whiskers of the box plot. Collagen fibre surface stiffness was not homogeneous throughout the sampled areas in each individual tissue type (Figure 3(b) and (c)). All three areas were statistically significant relative to each other ($p < 0.0001$).

High-contrast MPM imaging of collagen fibres

For illustration purposes, images from a single patient aged 42 years were representatively demonstrated (Figure 4). Collagen fibres were prominently visible within the dermis, whereas at the boundary of the dermal–epidermal junction (DEJ) very few SHG signals were present due to the absence of collagen within the epidermis.

In unscarred cellular dermis (Figure 4(a)–(c)), collagen fibres within the superficial and deep dermis had a random arrangement. Collagen fibres within scarred cellular dermis (Figure 4(g)–(i)) had an organised structural configuration of fibres. In the superficial dermis of scarred cellular dermis, the fibres were fragmented and aligned in a more parallel fashion relative to the epidermis below the basement membrane. Within the deep dermis, the fibres followed a longitudinal pattern. Decellularisation did not appear to affect the morphological characteristics of the dermal collagenous structure in both tissue types (comparing Figure 4(a)–(c) to (d)–(f), and Figure 4(g)–(i) to (j)–(l)).

The 3D images of collagen fibres were reconstructed from a region of interest in both superficial and deep dermis of cellular and decellularised tissue, originating from the same sample as in Figure 4, as depicted in Figure 5. Collagen fibres within unscarred cellular dermis were interwoven and more akin to a mesh-like structure (Figure 5(a) and (b)), whereas, in scarred cellular dermis, the fibres were parallel horizontally and vertically in the superficial and deep dermis, respectively (Figure 5(e) and (f)). Furthermore, decellularisation did not appear to alter the 3D dermal architecture as the native interwoven mesh structure was present in unscarred DCD, in both superficial and deep dermis (Figure 5(c) and (d)), and furthermore the horizontal and vertical alignment of fibres was observed in decellularised scarred superficial and deep dermis (Figure 5(g) and (h)), respectively.

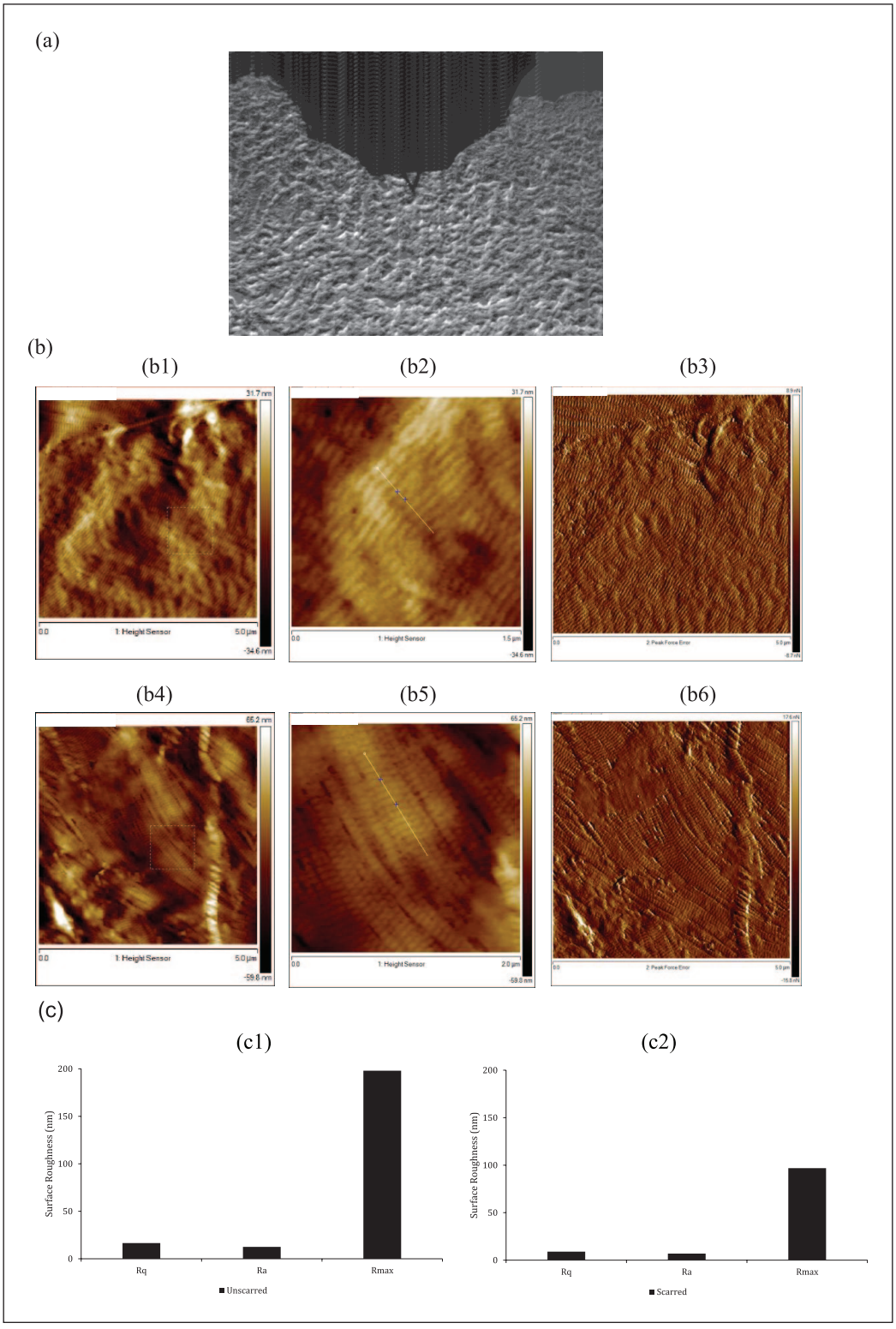

Figure 2. Surface topography of collagen fibres in unscarred and scarred decellularised dermis. (a) AFM optical image showing the location of the AFM cantilever in the scarred papillary dermis. (b) Tapping mode AFM images of decellularised unscarred (b1–b3) and scarred (b4–b6) dermis, using height contrast (b1–b4) and peak force error (b3, b6) taken at a depth of 100 μm below the epidermal basement membrane in the papillary dermis. It is possible to observe the orientation of the fibres 100 μm below the epidermal basement membrane in the papillary dermis. (b1, b4) 5 μm scan size. A 1.5-μm mask box is visible. (b2, b5) A higher resolution of 1.5 μm scan size, which is representative of the mask box. The *D*-period was analysed between two cross points along the straight line of a single collagen fibre. (c) AFM was used to calculate the surface roughness of collagen fibres in decellularised unscarred (c1) and scarred (c2) dermis between the two cross points in b2 and b5, using three common roughness parameters. AFM: atomic force microscopy; R_q: root mean square roughness; R_a: mean roughness; R_{max}: maximum roughness depth.

Table 3. Atomic force microscopy imaging structural analysis of collagen fibres in scarred and unscarred decellularised dermis.

	D-period (nm)	Standard deviation (nm)	Surface distance (nm)	Angle (°)	Thickness (nm)
Unscarred decellularised dermis	65	3.61	66	–3.2	154
Scarred decellularised dermis	69	2.49	71	–2.1	78

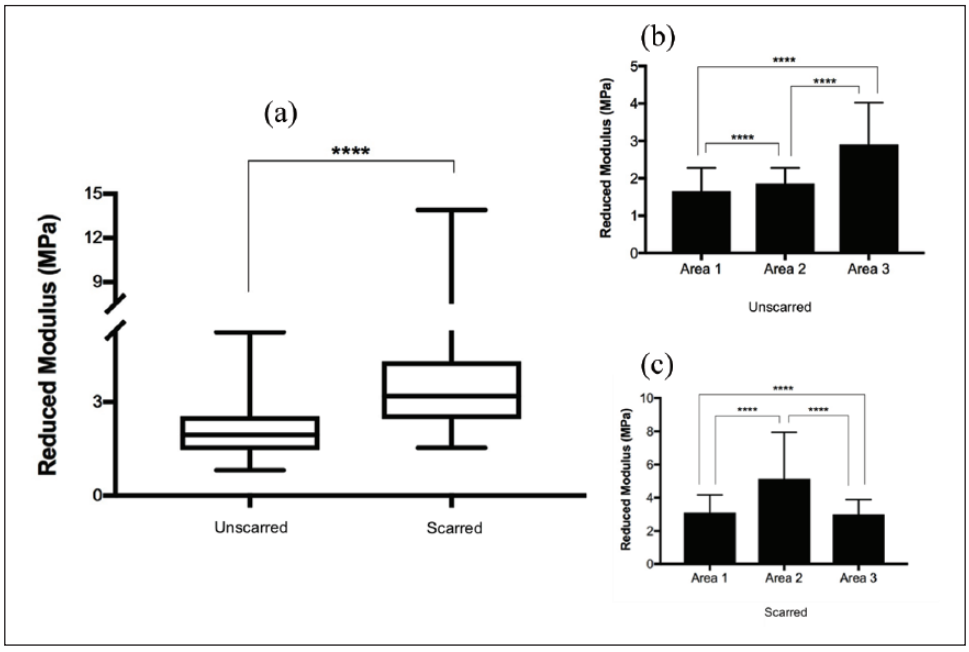

Figure 3. Mechanical analysis of collagen fibres in unscarred and scarred decellularised dermis. (a) A typical box and whisker plot demonstrating the variability in collagen fibre stiffness. (b, c) Collagen fibre stiffness was assessed in three individual areas for unscarred (b) and scarred (c) dermis. Results are presented as mean ± SD. (a) was analysed using paired *t*-test. (b) and (c) were analysed using both paired *t*-test and RM-OW-ANOVA.
****$p < 0.0001$.

Volume density of collagen

The volume density of collagen could represent well the excess deposition of collagen by fibroblasts during the wound healing process. It can be observed from Figure 5(i) and (j) that the volume densities of collagen for both unscarred and scarred dermis were similar before and after decellularisation.

Discussion

This study investigated the morphological structure of DCD in unscarred skin and its alteration in normal cutaneous scars. It has recently been established that the 3D arrangement of dermal tissue plays a crucial role in directing cellular behaviour during the wound healing process. Thus, for the purpose of advancing skin tissue engineering techniques for producing biomimetic materials for dermal regeneration, it is crucial to elucidate a better understanding of the 3D dermal architecture and its mechanical properties.

The decellularisation method used in this study was originally developed to decellularise a wide range of biological tissues.[18–21] The short duration of 5 days required for dermal decellularisation in this study is much shorter than the 25 cycles of decellularisation for over 40 days, which is necessary for certain tissues such as tracheal decellularisation with subsequent clinical implantation.[22] Decellularisation protocols shorter than 5 days have been described in the literature, especially for the neural retina and the retinal pigment epithelium.[23] In our study, the decellularisation method was appropriately amended and optimised several times in order to produce sufficient decellularisation of unscarred and scarred human dermis. Furthermore, to our knowledge, this is the first reported study of decellularisation of normotrophic scars in human skin.

A detailed histological analysis showed that hypotonic and detergent buffers in combination with enzymatic solutions and final storage in a tissue fixative or a –80°C freezer caused the removal of cells and maintained the native architectural characteristics of the dermal ECM.

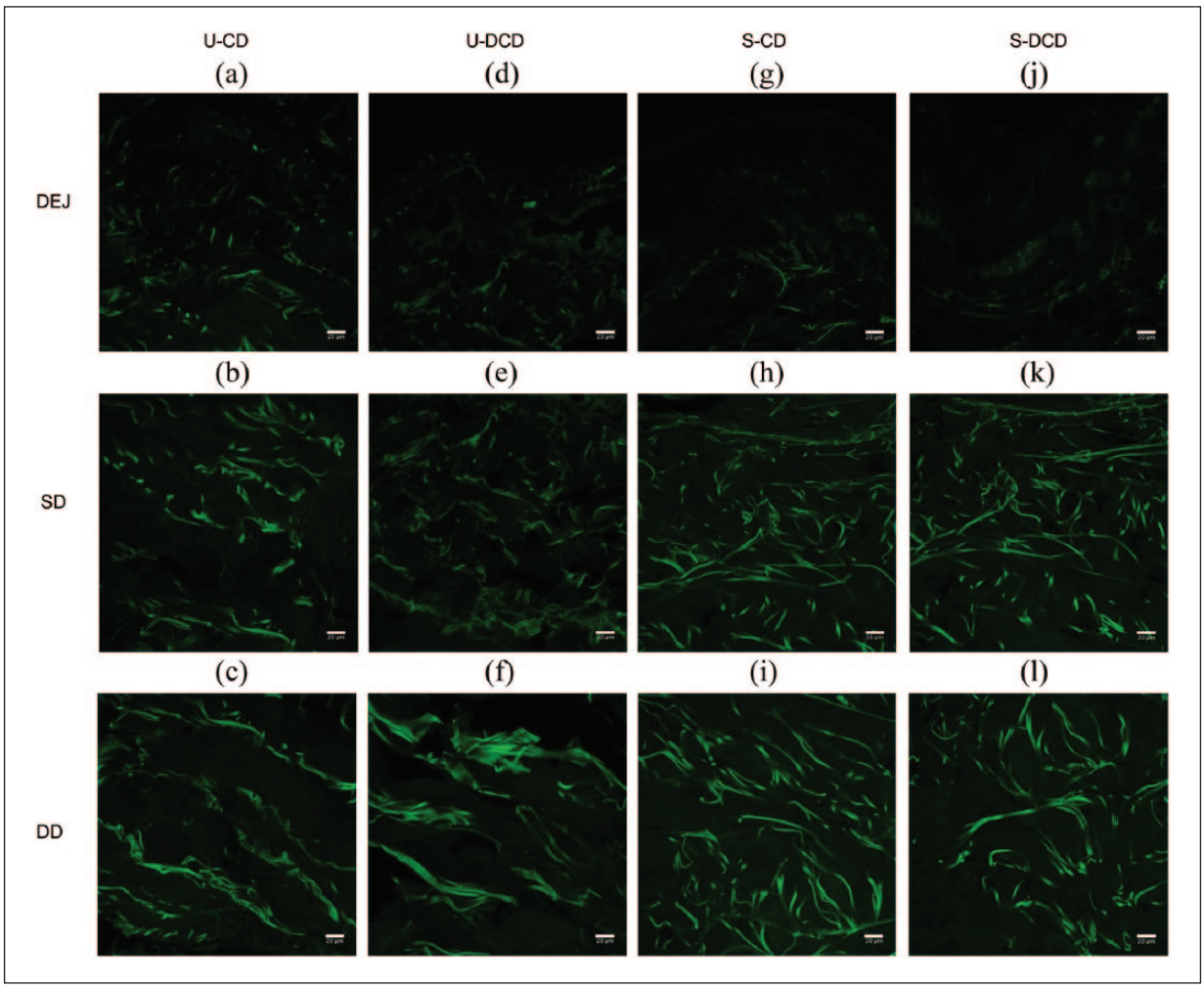

Figure 4. High-resolution 2D multiphoton images of collagen. High-resolution large-area SHG images (512 × 512 pixels, 8-bit) were obtained by MPM from unscarred and scarred dermis, both pre- and post-decellularisation. SHG images were extracted from the channel corresponding to wavelengths in the range of 398–409 nm, with an excitation wavelength of 810 nm and operating at 15% of maximum laser power. Images were obtained at differing levels across the longitudinal length of the sample. Images presented are from a single patient for ease of illustration. The 2D configuration of collagen fibers in unscarred (a-f) and scarred (g-l) dermis is visible by the intense green SHG signal. Few collagen fibers were visible at the DEJ of each specimen (a, d, g, j). Scale bars: 20 μm.
U-CD: unscarred cellular dermis; U-DCD: unscarred decellularised dermis; S-CD: scarred cellular dermis; S-DCD: scarred decellularised dermis; DEJ: dermal–epidermal junction; SD: superficial dermis; DD: deep dermis; MPM: multiphoton microscopy; SHG: second harmonic generation.

When compared to the control samples of intact skin, both unscarred and scarred dermis were successfully decellularised.

Structural changes were observed in unscarred and scarred DCD in our study. Following the remodelling stage of wound healing, there is a higher level of fibre organisation within the scarred tissue.[24] Cumming et al.[25] and Grant et al.[26] recently demonstrated an increased degree of collagen fibre orientation in scarred tissue. This is consistent with the results obtained in this study, where fibres of decellularised scarred dermis were more aligned relative to each other. Following cutaneous injury, the tensile strength of the scarred tissue is much lower than that of unscarred tissue. This may be related to the degree of fibre orientation observed in scarred tissue, as depicted in Figure 2(b4)–(b6). Both decellularised unscarred and scarred dermis exhibited low surface roughness overall (Figure 2(c)). A recent study demonstrated that surface topography can greatly influence the biological behaviour of cells.[13] Furthermore, in a related study, it was shown that biomaterials with rougher surfaces greatly enhanced fibroblast adhesion compared to a smoother surface.[27] As demonstrated in this study, there is a possibility that the lower roughness exhibited in scarred tissue can decrease fibroblast adhesion during the wound healing process. In addition, the lower surface roughness can greatly affect the phenotype of immune-modulatory cells in wound healing, especially macrophages, such that when macrophages

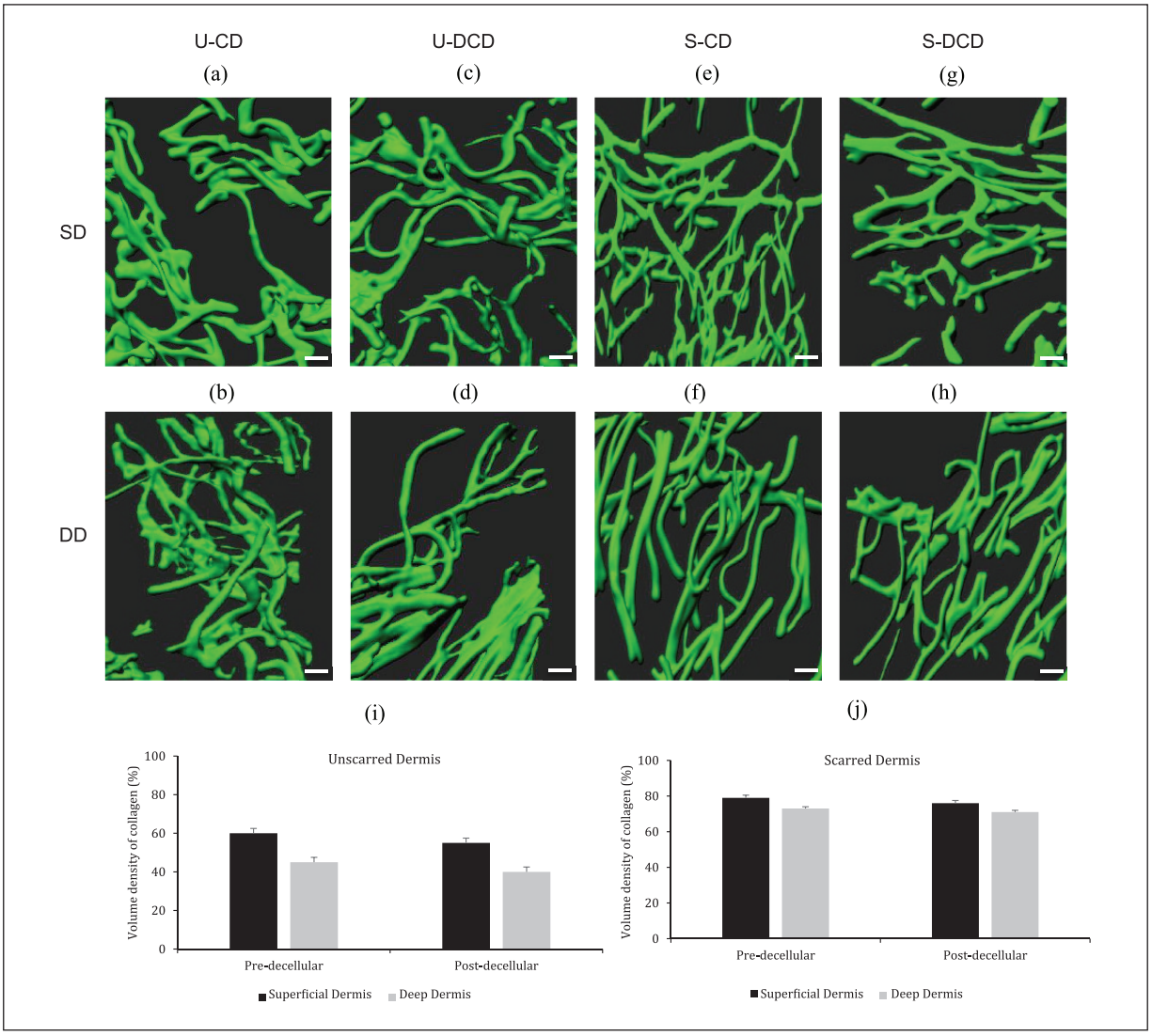

Figure 5. The 3D arrangement of collagen fibres in unscarred and scarred cellular and decellularised dermis and the corresponding volume densities. Shown are the representative morphological changes of collagen fibres from the papillary and reticular dermis in both samples. (a–h) 3D reconstruction of 2D images of cellular and decellularised dermis, originating from the same patient as shown in Figure 4. The 3D images correspond to the 2D images in Figure 4. (i, j) Collagen volume density was calculated using a standardised method for both unscarred (i) and scarred (j) dermis. Results are presented as mean ± SD. Scale bars: 10 μm.
U-CD: unscarred cellular dermis; U-DCD: unscarred decellularised dermis; S-CD: scarred cellular dermis; S-DCD: scarred decellularised dermis; SD: superficial dermis; DD: deep dermis.

contact a rough surface they are activated into a wound healing phenotype, whereas when contacting a smooth surface they can exhibit an inflammatory phenotype.[28] A closely related study assessed the nanomechanical properties of the ECM that influenced dermal fibroblast behaviour in different regions within the papillary and reticular dermis.[29] In their study, Achterberg et al.[29] found that, when a skin-soft culture substrate was used, fibroblasts exhibited a profile that was comparable to human dermis.

The collagen stiffness distribution data for decellularised scarred dermis appeared to have longer whiskers, which could be connected to regions where there is an increased collagen density resulting in higher elastic modulus values. AFM imaging cannot pick up this increased density of collagen, as subsurface anatomical structures are not clearly visualised. However, based on the MPM data (discussed below), increased collagen density is to be expected in scarred tissue.[25] From the surface roughness analysis, it is clear that the surface of collagen fibres is heterogeneous in nature. This itself could have accounted for the significant variation observed in the elastic modulus values. The cantilever tip may have contacted a rough peak on the surface resulting in a much larger indentation depth and thus a considerably higher elastic modulus value. Our reduced modulus of unscarred dermis was higher than that reported in a previously published study.[26] Furthermore, the

reduced modulus of scarred dermis was within the range described previously.[26] Although entirely speculative, it is possible that the decellularisation process could have affected the fibre stiffness of the unscarred dermis.

Using MPM, the morphology and quantity of collagen fibres in scarred tissue were analysed qualitatively and quantitatively, and compared to unscarred tissue. Our results show that this ECM component exhibits different morphologies in the superficial and deep dermis of unscarred and scarred tissue. Of particular interest is the direction of fibre orientation in scarred cellular and decellularised dermis. It is possible that the orientation of fibres within the scarred dermis likely followed the injury site due to their role in tissue repair and regeneration.[30] Despite the technological advances in dermatology, it still remains difficult to clearly distinguish between the superficial and deep dermis, as demonstrated by the overlap of longitudinal fibres in the lower half of the superficial dermis of scarred tissue. In addition, the collagen volume density analysis demonstrated an increase in collagen density in scarred tissue. This is however lower than that expected in pathological scarring.[31] This is an interesting finding, which correlates with our AFM data on the elastic modulus data for collagen fibres (mentioned above). We suggested that the wide range of elastic modulus measurements exhibited by decellularised scarred tissue might be related to areas of increased collagen density. It is important to highlight that our finding of increased collagen density, especially in deep dermis, is opposite to the results obtained by Zhu et al.[3]

There are some limitations to the methodology adopted in this study, namely, the fact that the age of scarred tissue was not clearly defined. We did not know the exact age of the scarred dermis, so it is not clear if comparison between scarred tissues of similar ages was being made. Second, only one static time point was analysed, therefore limiting our understanding of how the dermal collagenous structure alters with time during the wound healing process. In addition, our study lacks sample multiplicity beyond three samples each for both scarred and unscarred skin, primarily due to the difficulty in obtaining an adequate quantity of human tissue for multiple experiments. We hope that the findings of this preliminary work highlight the importance of informing tissue engineering research and development in the quest for finding optimal skin reliable skin substitutes and encourage further work to be undertaken. Finally, we were only able to achieve 88% and 90% cell removal for unscarred and scarred dermis, respectively. However, for the purposes of this study and because clinical transplantation of the DCD was not considered, we concluded and deemed that 88% and 90% cell removal was sufficient.

In conclusion, for the first time, decellularisation of scarred human dermis was achieved, which was evaluated using various techniques. The parameters addressed in this study should be carefully considered when developing engineered scaffolds for dermal wound repair. Ideally, based on unscarred DCD data, the scaffolds should exhibit a mesh-like structure with a rough surface and a low stiffness.

Acknowledgements

The Bioimaging Facility microscopes used in this study were purchased with grants from BBSRC, Wellcome and the University of Manchester Strategic Fund. Special thanks go to Steven Marsden for his help with the multiphoton microscope. We also thank Dr Nigel Hodson for his technical support with the atomic force microscope.

Author contributions

All contributors who did not meet the criteria for authorship have been listed in the Acknowledgments section. All authors gave consent for publication and made substantial contribution to the concept and design of the work as well as acquisition, analysis or interpretation of data; drafted the article or revised it critically for important intellectual content; and approved the final version to be published.

Declaration of conflicting interests

The author(s) declared no potential conflicts of interest with respect to the research, authorship and/or publication of this article.

Ethical approval

The relevant ethical committee (Human Tissue Authority) has provided approval and the approval number is stated in the section ‘Methods’.

Funding

The author(s) received no financial support for the research, authorship and/or publication of this article.

Informed consent

Patients provided written consent.

ORCID iD

Umair Khan https://orcid.org/0000-0002-4351-4058

References

1. Greaves NS, Ashcroft KJ, Baguneid M, et al. Current understanding of molecular and cellular mechanisms in fibroplasia and angiogenesis during acute wound healing. *J Dermatol Sci* 2013; 72(3): 206–217.
2. Atiyeh BS, Costagliola M and Hayek SN. Keloid or hypertrophic scar: the controversy: review of the literature. *Ann Plast Surg* 2005; 54(6): 676–680.
3. Zhu X, Zhuo S, Zheng L, et al. Quantified characterization of human cutaneous normal scar using multiphoton microscopy. *J Biophotonics* 2010; 3(1–2): 108–116.
4. Jiang Y and Lu S. Exploring the dermal ‘template effect’ and its structure. *Mol Biol Rep* 2013; 40(8): 4837–4841.
5. Lu SL, Qin C, Liu YK, et al. [Study on the mechanism of scar formation: epidermis template defect theory]. *Zhonghua Shao Shang Za Zhi* 2007; 23(1): 6–12.

6. Kanitakis J. Anatomy, histology and immunohistochemistry of normal human skin. *Eur J Dermatol* 2002; 12(4): 390–399; quiz 400–401.
7. Provenzano PP, Inman DR, Eliceiri KW, et al. Contact guidance mediated three-dimensional cell migration is regulated by Rho/ROCK-dependent matrix reorganization. *Biophys J* 2008; 95(11): 5374–5384.
8. Ma PX. Biomimetic materials for tissue engineering. *Adv Drug Deliv Rev* 2008; 60(2): 184–198.
9. Yasui T, Tohno Y and Araki T. Characterization of collagen orientation in human dermis by two-dimensional second-harmonic-generation polarimetry. *J Biomed Opt* 2004; 9(2): 259–264.
10. Jiang Y, Tong Y and Lu S. Visualizing the three-dimensional mesoscopic structure of dermal tissues. *J Tissue Eng Regen Med* 2014; 8(10): 794–800.
11. Boyce ST. Design principles for composition and performance of cultured skin substitutes. *Burns* 2001; 27(5): 523–533.
12. Supp DM and Boyce ST. Engineered skin substitutes: practices and potentials. *Clin Dermatol* 2005; 23(4): 403–412.
13. Jiang Y and Lu S. Three-dimensional insights into dermal tissue as a cue for cellular behavior. *Burns* 2014; 40(2): 191–199.
14. Mazza G, Rombouts K, Hall AR, et al. Decellularized human liver as a natural 3D-scaffold for liver bioengineering and transplantation. *Sci Rep* 2015; 5: 13079.
15. Occleston NL, O'Kane S, Goldspink N, et al. New therapeutics for the prevention and reduction of scarring. *Drug Discov Today* 2008; 13(21–22): 973–981.
16. Tebble NJ, Thomas DW and Price P. Anxiety and self-consciousness in patients with minor facial lacerations. *J Adv Nurs* 2004; 47(4): 417–426.
17. Newell R. Psychological difficulties amongst plastic surgery ex-patients following surgery to the face: a survey. *Br J Plast Surg* 2000; 53(5): 386–392.
18. Booth C, Korossis SA, Wilcox HE, et al. Tissue engineering of cardiac valve prostheses I: development and histological characterization of an acellular porcine scaffold. *J Heart Valve Dis* 2002; 11(4): 457–462.
19. Wilcox HE, Korossis SA, Booth C, et al. Biocompatibility and recellularization potential of an acellular porcine heart valve matrix. *J Heart Valve Dis* 2005; 14(2): 228–236; discussion 236–237.
20. Wilshaw SP, Rooney P, Berry H, et al. Development and characterization of acellular allogeneic arterial matrices. *Tissue Eng Part A* 2012; 18(5–6): 471–483.
21. Wilshaw SP, Kearney JN, Fisher J, et al. Production of an acellular amniotic membrane matrix for use in tissue engineering. *Tissue Eng* 2006; 12(8): 2117–2129.
22. Macchiarini P, Jungebluth P, Go T, et al. Clinical transplantation of a tissue-engineered airway. *Lancet* 2008; 372(9655): 2023–2030.
23. Dorgau B, Felemban M, Hilgen G, et al. Decellularised extracellular matrix-derived peptides from neural retina and retinal pigment epithelium enhance the expression of synaptic markers and light responsiveness of human pluripotent stem cell derived retinal organoids. *Biomaterials* 2019; 199: 63–75.
24. Dallon JC, Sherratt JA and Maini PK. Mathematical modelling of extracellular matrix dynamics using discrete cells: fiber orientation and tissue regeneration. *J Theor Biol* 1999; 199(4): 449–471.
25. Cumming BD, McElwain DL and Upton Z. A mathematical model of wound healing and subsequent scarring. *J R Soc Interface* 2010; 7(42): 19–34.
26. Grant CA, Twigg PC and Tobin DJ. Static and dynamic nanomechanical properties of human skin tissue using atomic force microscopy: effect of scarring in the upper dermis. *Acta Biomater* 2012; 8(11): 4123–4129.
27. Valencia-Lazcano AA, Alonso-Rasgado T and Bayat A. Characterisation of breast implant surfaces and correlation with fibroblast adhesion. *J Mech Behav Biomed Mater* 2013; 21: 133–148.
28. Barth KA, Waterfield JD and Brunette DM. The effect of surface roughness on RAW 264.7 macrophage phenotype. *J Biomed Mater Res A* 2013; 101(9): 2679–2688.
29. Achterberg VF, Buscemi L, Diekmann H, et al. The nanoscale mechanical properties of the extracellular matrix regulate dermal fibroblast function. *J Invest Dermatol* 2014; 134(7): 1862–1872.
30. Riemann I, Ehlers A, LeHarzic R, et al. In vivo multiphoton tomography of skin during wound healing and scar formation. *Proc SPIE* 2007; 6442: 644226.
31. Chen J, Zhuo S, Jiang X, et al. Multiphoton microscopy study of the morphological and quantity changes of collagen and elastic fiber components in keloid disease. *J Biomed Opt* 2011; 16(5): 051305.